UC San Diego
UC San Diego Previously Published Works

Title

Caenorhabditis elegans Egg-Laying Detection and Behavior Study Using Image Analysis

Permalink

https://escholarship.org/uc/item/6qm0v9jn

Journal

EURASIP Journal on Advances in Signal Processing, 2005(14)

ISSN

1687-6172 1687-6180

Authors

Geng, Wei
Cosman, Pamela
Palm, Megan
et al.

Publication Date

2005

DOI

10.1155/ASP.2005.2229

Peer reviewed

Caenorhabditis elegans Egg-Laying Detection and Behavior Study Using Image Analysis

Wei Geng

Department of Electrical and Computer Engineering, University of California at San Diego, La Jolla, CA 92093-0407, USA
Email: wei_geng@yahoo.com

Pamela Cosman

Department of Electrical and Computer Engineering, University of California at San Diego, La Jolla, CA 92093-0407, USA
Email: pcosman@code.ucsd.edu

Megan Palm

Division of Biological Sciences, University of California at San Diego, La Jolla, CA 92093-0349, USA
Email: mpalm@ucsd.edu

William R. Schafer

Division of Biological Sciences, University of California at San Diego, La Jolla, CA 92093-0349, USA
Email: wschafer@ucsd.edu

Egg laying is an important phase of the life cycle of the nematode *Caenorhabditis elegans (C. elegans)*. Previous studies examined egg-laying events manually. This paper presents a method for automatic detection of egg-laying onset using deformable template matching and other morphological image analysis techniques. Some behavioral changes surrounding egg-laying events are also studied. The results demonstrate that the computer vision tools and the algorithm developed here can be effectively used to study *C. elegans* egg-laying behaviors. The algorithm developed is an essential part of a machine-vision system for *C. elegans* tracking and behavioral analysis.

Keywords and phrases: egg-laying, *C. elegans*, behaviors, image analysis, deformable template matching, computer vision.

1. INTRODUCTION

The nematode *Caenorhabditis elegans (C. elegans)* is widely used for genetic studies of development, cell biology, and gene regulation. In particular, because of its facile genetics, well-described nervous system, and complete genome sequence, it is particularly well suited to analysis of the molecular and cellular basis of nervous system function and development. The ability to functionally map the influence of particular genes to specific behavioral phenotypes makes it possible to use genetic analysis to functionally dissect the molecular mechanisms underlying poorly understood aspects of nervous system function such as addiction, learning, and

sensory perception. However, many genes with critical roles in neuronal function have effects on behavior that are difficult to describe precisely, or occur over time scales too long to be compatible with real-time scoring by a human observer. Therefore, to fully realize the potential of *C. elegans* for the genetic analysis of the nervous system function, it is necessary to develop sophisticated methods for the rapid and consistent quantitation of mutant phenotypes, especially those related to behavior.

One of the most important behaviors for the analysis of neuronal signal transduction mechanisms is egg laying. Egg laying in *C. elegans* occurs when embryos are expelled from the uterus through the contraction of 16 vulval and uterine muscles [1]. In the presence of abundant food, wild-type animals lay eggs in a specific temporal pattern: egg-laying events tend to be clustered in short bursts, or active phases, which are separated by longer inactive phases during

which eggs are retained. This egg-laying pattern can be accurately modeled as a three-parameter probabilistic process in which animals fluctuate between discrete inactive, active, and egg-laying states [2]. Egg laying has also been shown to be coordinated with locomotion: specifically, animals undergo a transient increase in global speed immediately before each egg-laying event [3]. Many neurotransmitters and neuronal signal transduction pathways have been shown to have specific effects on egg-laying behavior; thus it has become an important behavioral assay for the analysis of many neurobiological problems in *C. elegans*.

Computer vision tools [4, 5, 6] have been used successfully in recording, tracking, defining, and classifying *C. elegans* morphology and locomotion behaviors. Because egg laying is infrequent, it is well suited for analysis by automated imaging methods. In previous egg-laying studies [2, 3, 7, 8], individual worm movements were videotaped and the centroid location and time information were saved at 1-second intervals during recording. The entire videos were later played back and each video frame was examined by expert observers to look for egg and egg onset frames. In this paper, we present an algorithm that can identify eggs and egg onsets automatically. In addition, by combining this information with the features (locomotion, morphology, behavior, shape) extracted using our previously developed computer vision methods, we are able to uncover relationships between egg-laying events and other characteristics.

2. IMAGE ACQUISITION AND SEGMENTATION

2.1. Acquisition of the video images

Routine culturing of *C. elegans* was performed as described in [9]. All worms analyzed in these experiments were young adults; fourth-stage larvae were picked the evening before the experiment and tracked the following morning after cultivation at 22°. All animals used in this study were from the wild-type Bristol (N2) strain.

C. elegans locomotion was tracked with a stereomicroscope mounted with a CCD video camera [4, 5, 6]. The video camera used only a single eyepiece, and so did not have stereo data; the system is equivalent to a conventional brightfield microscope. A computer-controlled tracker was used to maintain the worms in the center of the optical field of the microscope during observation. To record the locomotion of an animal, an image frame of the animal was snapped every 0.5 second for at least five minutes (20 minutes or more in the longer recordings). Among those image pixels with values less than or equal to the average value minus three times the standard deviation, the largest connected component was found. The image was then trimmed to the smallest axis-aligned rectangle that contained this component, and saved as eight-bit grayscale data. The dimensions of each image and the coordinates of the upper-left corner of the bounding box surrounding the image were also saved simultaneously as the references for the location of an animal in the tracker field at the corresponding time point when the images are snapped. The microscope was fixed to its largest magnification (50 X)

during operation. Depending on the type and the posture of a worm, the number of pixels per trimmed image frame varied. The number of pixels per millimeter was fixed at 312.5 pixel/mm for all worms.

2.2. Segmentation and tracking of the worm body

The segmentation process is presented in [6]. Briefly, an adaptive local thresholding algorithm with a 5×5 moving window was used followed by a morphological closing operator (binary dilations followed by erosions). A corresponding reference binary image was also generated by filling the holes inside a worm body based on image content information. The difference between these two binary images provided a good indication of which image areas are worm body and which are background.

Following binarization, a morphological skeleton was obtained by applying a skeletonizing algorithm. Redundant pixels on the skeleton were eliminated by thinning. To avoid branches on the ends of skeletons, the skeleton was first shrunk from all its end points simultaneously until only two end points were left. These two end points represent the longest end-to-end path on the skeleton. A clean skeleton can then be obtained by growing out these two remaining end points along the unpruned skeleton by repeating a dilation operation.

The tracking algorithm is presented in [6], and included automatic recognition of the head and tail for the worm inside each frame.

3. MODEL-BASED ATTACHED EGG DETECTION

3.1. Image analysis

To find the possible egg locations and limit the search area for deformable template matching, we developed a series of morphological image analysis algorithms to limit our search area to around 2% of a typical region that a worm body covers. The search is greatly expedited and match accuracy is improved by effectively eliminating potential false alarms. The flowchart of attached egg detection is shown in Figure 1. For each input video frame, the worm body is first segmented from the background and the skeleton (medial axis) is obtained by algorithms described in [6]. The laying of an egg changes the shape of the binarized worm body (Figure 2), which can be captured by examining the width profile in the middle part of the worm body in the following way. For each pixel in the skeleton pixel list, a straight line traversing the worm body that passes through that skeleton pixel is calculated. Seventy one additional lines are also calculated at 5-degree intervals to cover a 360-degree radius. The worm body width at that skeleton pixel is the shortest of the 72 lines, which has the shortest distance traversing the binary image through the skeleton pixel. In the case where the abnormal width is caused by an attached egg, one of the two end point locations on the shortest-distance line is enclosed by that egg. By abnormal width, we mean a difference greater than 7.5 pixels/24 μm between median and peak width in the middle part of the body, indicating a
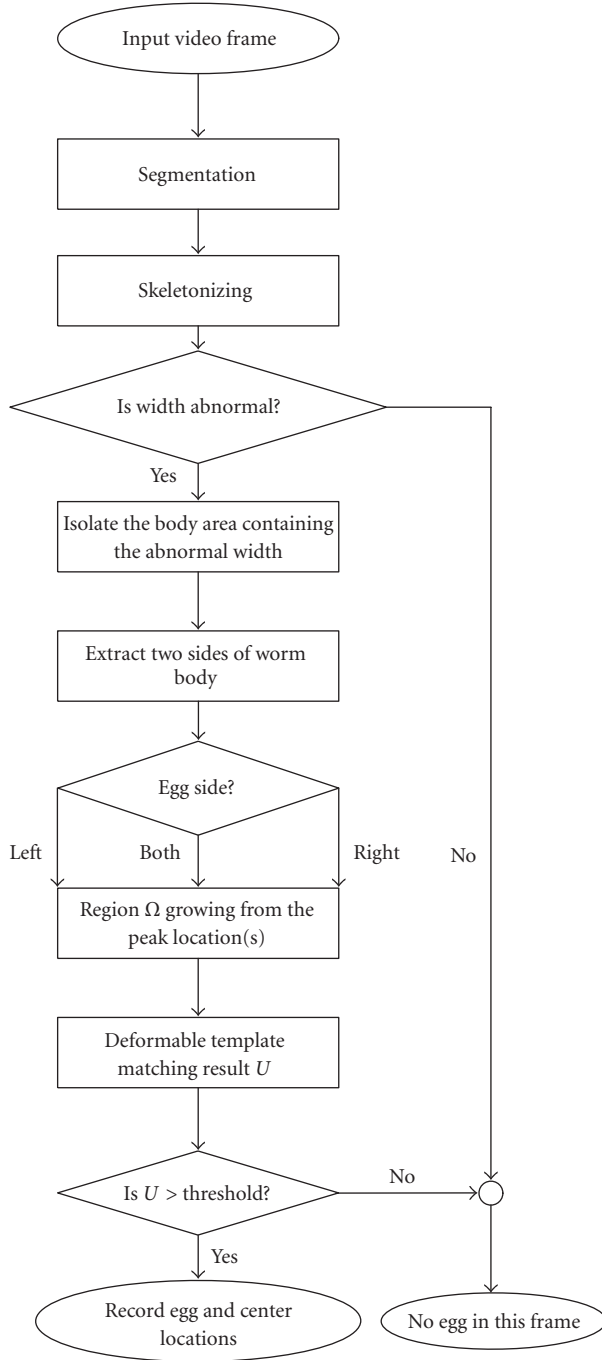
FIGURE 1: Flowchart of the egg detection process.

potential egg event. Figure 2a shows the frame immediately prior to an egg-laying event. Figure 2b shows the egg-laying frame. The corresponding width profiles are shown in Figures 2c and 2d, respectively. The solid curves show the width measured along the worm skeletons. The horizontal dotted lines in Figures 2c and 2d show the median width for the middle part of the worm body. A second horizontal line in Figure 2d shows the threshold (7.5 pixels above the median width value) that defines abnormal width. The width-profile

curves are normalized to 300 pixels for comparison. Since egg laying is a rare event, over 90% of the frames are quickly passed through and not subject to further analysis.

Since the abnormal width measure cannot tell us on which side the egg is (which end point the egg encloses), we extract the boundary from both sides of the worm body and consider the side that has higher k-curvature values to be the egg side. This way, the search area is constrained to only one side of the worm body and half of the search area is effectively eliminated. The process starts with isolating the body area containing the abnormal width by cutting off the worm body area, that is, 25 pixels/80 μm before and after using the minimal-distance straight lines passing through the skeleton pixels. This cutoff area is 51 pixels/160 μm in medial axis and has four boundaries. Two of the boundaries are the straight cutoff lines, and the other two are the two sides of the worm body (Figure 3b). A boundary-following algorithm similar to the one in [10] is then used to extract the two boundaries along the sides of the worm body (Figure 3c). The k-curvature ($k = [3, 7]$) [11] of these two boundaries is calculated, and the boundary that has higher (for all 5 k-curvature measurements) values is designated as the egg side. If neither boundary has all the 5 measurements higher, both sides are checked for eggs. The k-curvature is defined as $R = \{(1/(n-1)) \sum_{i=1}^{n-1} \theta_i\}$, where

$$\theta_i = \arctan \frac{y_{i+2} - y_{i+1}}{x_{i+2} - x_{i+1}} - \arctan \frac{y_{i+1} - y_i}{x_{i+1} - x_i}, \qquad (1)$$

and (x_i, y_i), (x_{i+1}, y_{i+1}),... are the locations of consecutive points that are k pixels apart along the worm side boundaries.

Once the location of the maximal peak is decided, the search region Ω can be obtained by the region growing out of the egg-side end point to enclose the egg center. A directional dilation algorithm such as the one in [12] can be used for this purpose. Here we once again take advantage of the worm skeleton. The directional dilation is achieved by applying two constraints in the dilation process: (1) dilation starts from the end point and should remain inside the binary worm body; (2) dilation remains outside skeleton area (dilated 4 times from skeleton) (Figure 3d). The dilation process stops when more than 200 pixels are inside the region. The directional dilation forces the search area to be inside the worm body close to the side boundaries rather than close to the skeleton. The final search region Ω (Figure 3e) typically contains between 200 and 250 pixels for each frame. In the case that both sides are checked, a total of 400 pixels is checked. Figure 3 illustrates the process.

3.2. Deformable template matching

Deformable template matching models have been applied to a variety of image recognition and analysis applications with success [13, 14, 15, 16, 17]. They not only enjoy the flexibility of a parameterized model, but also can be explained in a Bayesian framework. Even though the attached eggs could be partially obscured by shadows and/or by the worm body, or partially laid, they share many common characteristics.
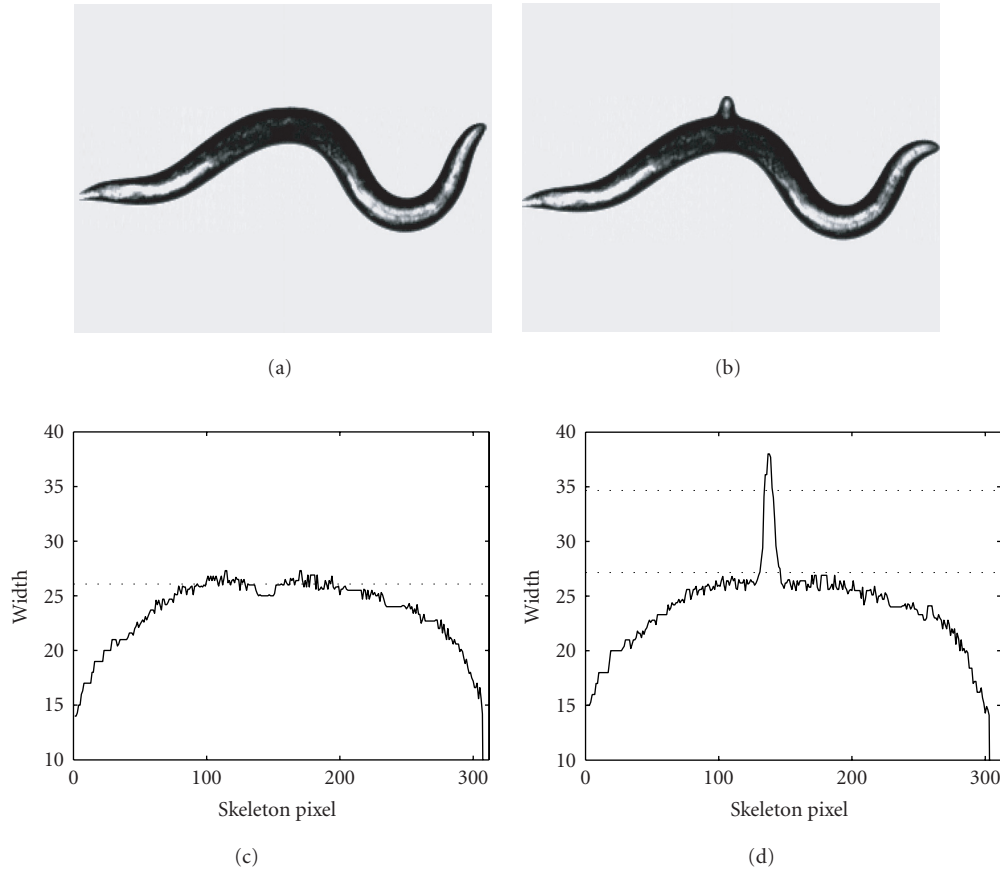
(a)

(b)

(c)

(d)

FIGURE 2: Width profile change on egg onset. (a) Gray image right before egg onset. (b) Gray image right after egg onset. (c) Width profile of (a). The dotted line is the median value of the middle part of the width profile. (d) Width profile of (b). The lower dotted line is the median value of the middle part of the width profile. The upper dotted line is 7.5 pixels above the lower dotted line.

They tend to have oval shapes, and are generally brighter in the middle and darker around the boundary. The eggs are more or less similar in size. These characteristics make them ideal for the elliptic deformable templates.

In an ideal case, the shape of the attached eggs can be modeled by an elliptic model such as the one shown in Figure 4 with 7 parameters $v = (x, y, a, b, \theta, \rho1, \rho2)$, where (x, y) are the coordinates of the center, a and b are the semi-axes, and θ is the rotation angle. Together, these 5 parameters control the geometric shape and location of the inner ellipse that captures the bright center part of the egg. $\rho1$ equals the ratio between the area of the middle band and the inner ellipse, $\rho2$ equals the ratio between the area of the outer band and the middle ellipse. The middle band encloses the dark exterior part of the egg. The outer band covers part of the worm body and part of the background. By studying the homogeneity of the pixels enclosed, the outer band can be used to suppress noise and find the best location for the egg. For example, if (x, y) is mistakenly inside the worm body, then the outer band will have similar brightness to the worm body (dark). If (x, y) is in the background area, the outer band has similar brightness to the background (light). Half worm body and half background inside the outer band indicate

a perfect attached egg location. To reduce model complexity, we opt to use a simplified model (Figure 5) that does not have the outer band, and use image analysis to restrain the search area. The outer band in Figure 4 is only used for deletion purposes when multiple eggs/peaks are detected. In these cases, the pixels inside the entire outer ellipse are deleted and the process is repeated to detect additional eggs. The outer band is also shown in Figures 3, 7, and 8 to mark the location of the best-fit ellipse. There are 6 parameters characterizing the shape of the simplified elliptic model $v = (x, y, a, b, \theta, \rho)$.

From a Bayesian framework, we have $p(v|E) = p(v)p(E|v)/p(E)$, where E is the event that the image contains an egg, and $p(v|E)$ is the probability density function of parameter configuration given that an egg is present. There are many ways to define the likelihood function. We propose the following model:

$$p(E|v) = \frac{1}{z} \exp \left\{ - \left(\alpha \mu_{\text{in}}(v) + \beta \mu_{\text{out}}(v) \right) \right\}, \qquad (2)$$

where $\mu_{\text{in}}(v)$ is the mean pixel value inside the inner ellipse, $\mu_{\text{out}}(v)$ is the mean pixel value in the band around the inner ellipse (Figure 5), and α, β are weights to be selected to give

(a)

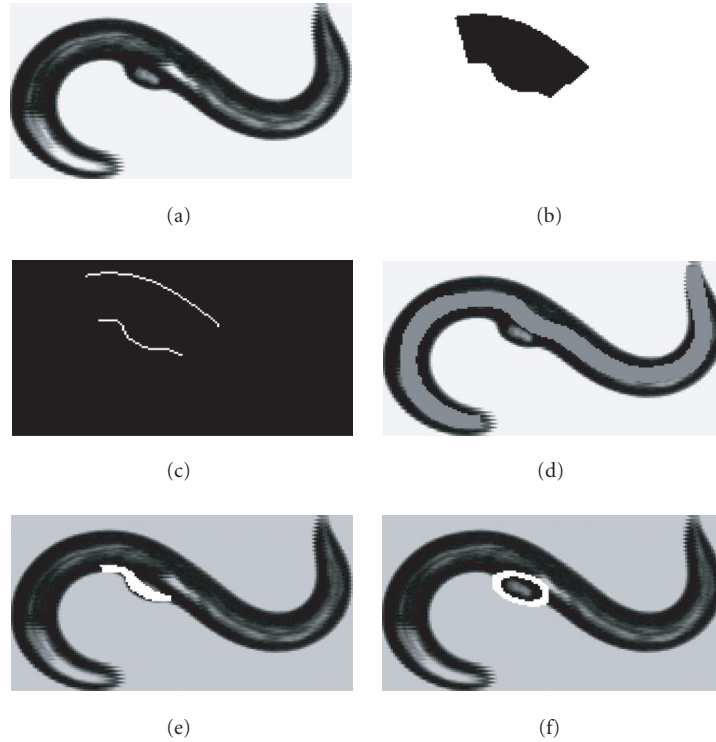(b)

(c)

(d)

(e)

(f)

FIGURE 3: Illustration of egg-detection image analysis. (a) Grayscale image. (b) The cutoff portion containing egg. (c) Two boundaries. (d) The highlighted area (gray) shows the dilation of the skeleton four times. This area is not searched for eggs. (e) The highlighted area (white) shows final search region. (f) Best-fit ellipse.
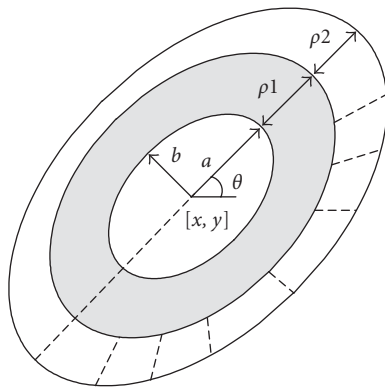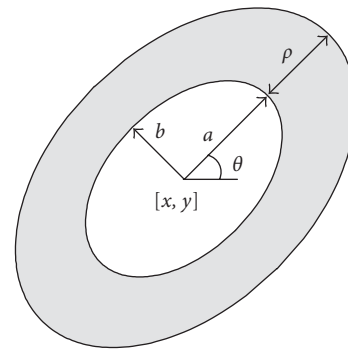

FIGURE 4: Ellipse egg model.

FIGURE 5: Simplified ellipse egg model.

a proper weight for inside and outside areas. For calculating the mean values, the pixel intensities are linearly rescaled to go from -1 to $+1$. z is a normalization constant to ensure that $p(E|v)$ is a proper probability density of unit area.

The egg-finding problem can then be modeled as finding the most likely parameter configuration v_{opt} given that there is an egg in the image. Using a maximum a posteriori (MAP) estimator,

$$v_{\text{opt}} = \arg_v \max p(v|E) = \arg_v \max \frac{p(v)p(E|v)}{p(E)}. \quad (3)$$

Since the egg can occur in any orientation and location in the search space, it is reasonable to assume a uniform prior. For simplicity, we also assume that a and b are uniformly distributed in a narrow range. So (3) is identical to

$$
\begin{aligned}
v_{\text{opt}} &= \arg_v \max p(E|v) \\
&= \arg_v \max \frac{1}{z} \exp\left\{-\left(\alpha \mu_{\text{in}}(v) + \beta \mu_{\text{out}}(v)\right)\right\}.
\end{aligned} \quad (4)
$$

Furthermore, because z is a constant, and we can absorb the minus sign into the parameters α and β, (4) is identical to

$$v_{\text{opt}} = \arg_v \max \left\{\alpha \mu_{\text{in}}(v) + \beta \mu_{\text{out}}(v)\right\}. \quad (5)$$
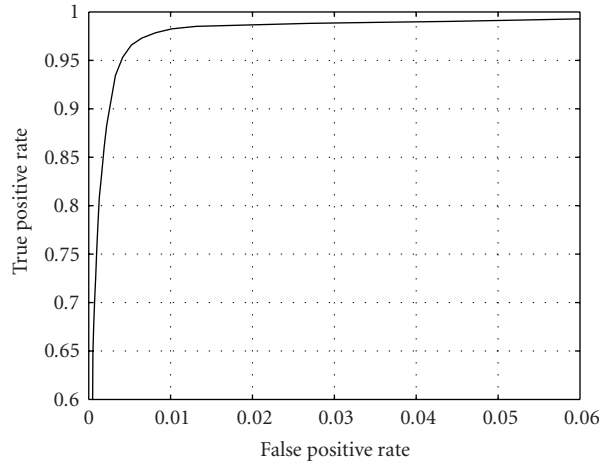
FIGURE 6: A plot of the receiver operating characteristic (ROC) curve with threshold t varying from -1.5 to 1.5.

The optimal parameter configuration is the parameter ν that maximizes the function

$$U(\nu) = \alpha\mu_{\text{in}}(\nu) + \beta\mu_{\text{out}}(\nu). \tag{6}$$

We chose $\alpha = 0.5$, $\beta = -1$, and $\rho = 8$ by feeding a small set of training samples of egg and nonegg values of μ_{in}, μ_{out} into the classification and regression tree (CART) algorithm [18]. The final model for locating eggs is as follows.

For a specified search space Ω in the image, find

$$\nu_{\text{opt}} = (x_{\text{opt}}, y_{\text{opt}}, a_{\text{opt}}, b_{\text{opt}}, \theta_{\text{opt}}) = \arg_\nu \max U(\nu), \tag{7}$$

where $U = 0.5\mu_{\text{in}}(\nu) - \mu_{\text{out}}(\nu)$. Notice $U \in [-1.5, 1.5]$.

For every pixel (x_c, y_c) inside the search region Ω, U is calculated for each configuration with a range ($a = [3.4, 3.6]$, $b = [1.9, 2.1]$, $\theta = [0, 180]$). If U_{opt} is greater than a threshold value t, the location $(x_{\text{opt}}, y_{\text{opt}})$ is marked as the egg location and an egg is declared found.

3.3. Experimental results

The egg detection algorithm was tested on 1 600 5-minute video sequences from 16 different mutant types (100 videos for each type) and five 20-minute video sequences of wild-type animals treated with serotonin, which causes an increase in egg laying. The data were collected over a 3-year period by different individuals. A laborious manual check found 9 000 frames containing 200 different eggs. These eggs cover a wide variety of recording conditions, mutant types, sizes, and shapes. 100 000 nonegg frames were randomly selected from the rest of the 800 000 frames as nonegg cases. By applying the above algorithm with the decision threshold t varying from -1.5 to 1.5, the performance result is shown as an ROC curve [19] in Figure 6 and Table 1. The true positive fraction is over 98% when the false positive fraction is 1%. Figure 7 shows some examples of the locations and best-fit ellipses identified by the algorithm. Some failure examples are shown in Figure 8.

4. EGG ONSET DETECTION AND BEHAVIOR STUDY

4.1. Egg onset detection

Egg detection algorithms can be readily incorporated into a broader scheme for egg onset event detection (identifying the frames in which the egg first appears). Figure 9 shows one algorithm to accomplish it. The main functions of the egg onset detection routine are to use the single-frame egg detection result for a sequence. First, we decide whether the current egg is a newly laid or a previously laid egg (worms sometimes crawl back to previous eggs). This is accomplished by maintaining a list of all existing locations of eggs. When the new location is not on the list, an egg onset event is detected. Secondly, there are occasions when multiple eggs are laid at the same time. Also, there are cases when multiple width abnormalities are detected for a single frame due to multiple newly laid and previous laid eggs that remain near the worm body. The egg onset detection routine runs the single-frame egg detection routine repeatedly in the search regions after the detected egg area (outer ellipse in the template model) is removed from the image in each run. This way, clusters of eggs can be detected. The egg onset detection routine also runs the abnormal width detection routine repeatedly to find out new search regions to detect all the eggs attached to the worm body.

The onset detection algorithm was tested on 25 videos of 20-minute recordings (500 minutes, 60 000 total frames). These recordings include 5 serotonin videos previously used for the egg detection test and 20 new normal wild-type videos. By setting the thresholds conservatively ($t = 0.5$) and declaring that an egg onset has occurred if one or more new eggs are detected in three or more consecutive frames, our algorithm is able to pick up all 88 egg onsets in one pass through the videos. There are 131 false-alarm onset frames for the entire data set of 60 000 frames. The false-alarm onsets are easily eliminated by inspecting each onset frame visually. Among the 88 onsets detected, there are 6 onsets that are delayed from true onsets by 1, 2, 3, 4, 10, 18 frames, respectively.

TABLE 1: The false positive, true positive, false negative, and true negative values for part of the ROC curve. The boldface row is the final threshold used in the egg onset detection.

Rate of nonegg frames detected as egg (false positive)	Rate of egg frames detected as egg (true positive)	Rate of egg frames detected as nonegg frames (false negative)	Rate of nonegg frames detected as nonegg frames (true negative)	Threshold t
0.0967	0.9985	0.0015	0.9033	0.35
0.0947	0.9983	0.0017	0.9053	0.36
0.0924	0.998	0.002	0.9076	0.37
0.0893	0.9977	0.0023	0.9106	0.38
0.0857	0.9972	0.0028	0.9143	0.39
0.0814	0.9964	0.0036	0.9186	0.4
0.0769	0.9961	0.0039	0.9231	0.41
0.072	0.9955	0.0045	0.928	0.42
0.0663	0.9946	0.0054	0.9337	0.43
0.0597	0.9927	0.0073	0.9403	0.44
0.0524	0.9915	0.0085	0.9476	0.45
0.044	0.9902	0.0098	0.956	0.46
0.0354	0.9893	0.0107	0.9646	0.47
0.027	0.9883	0.0117	0.973	0.48
0.0194	0.9865	0.0135	0.9806	0.49
0.0131	**0.9851**	**0.0149**	**0.9869**	**0.5**
0.0101	0.9826	0.0174	0.9899	0.51
0.0082	0.9785	0.0215	0.9918	0.52
0.0065	0.9729	0.0271	0.9935	0.53
0.0052	0.9658	0.0342	0.9948	0.54
0.0042	0.9531	0.0469	0.9959	0.55

4.2. Behavior study

Previous study [3] indicated significantly increasing locomotion activity prior to egg onset. We studied the behavior changes before and after 55 wild-type egg onsets (a fresh 10-hour recording) detected by our onset detection algorithm. The behavioral characteristics can be summarized by extracting features proposed by the feature extraction system [4, 5, 6]. For each feature, we looked for a significant difference in that feature before and after the onset frame by using the nonparametric rank sum test on paired data. For each of the 55 eggs, we paired the data obtained from the 40 seconds before the onset frame with data after the onset frame. The 253 features examined include 131 morphological features (thickness, fatness, MER, angle change rate, etc.), 75 speed features (min, max, average speed over 1, 5, 10, 20, 30, 40 seconds, etc.), 35 texture features (head, tail, center brightness, etc.), and 12 other behavioral features (rate of reversals, omega shape, looping, etc.). Out of these 253 features, 14 were found to be significant at the 0. 01 significance level as shown in Table 2. We also considered the possibility that some features may be significantly different both before and after egg laying compared to the values for a worm that is not near an egg-laying time. So we also looked at the paired data where the values obtained from the 40 seconds before an egg-laying onset were paired with the values from an equal number of frames starting from a randomly

selected nonegg frame, and similarly where the values after an egg-laying onset were paired with the values from an equal number of frames starting from a randomly selected nonegg frame. There were 32 (Table 3) comparisons that were significant at the 0. 01 significance level before egg onset and 32 after, respectively. We note that, by random chance alone, out of 253 comparisons, we would expect to see 2.5 features showing a significant difference at the 0. 01 significance level.

Most of the features found to be significantly different were related to speed, confirming earlier results that were determined manually. In particular, we found that the global centroid movement as well as the local movement of the tail and head were all significantly larger before the onset compared to after (see Figure 10). Previous results only considered global movement. Local head movement is often related to foraging behavior. We also found some differences in brightness parameters. Due to the multiplicity of comparisons being made, these remain to be verified when further data are collected.

5. CONCLUSION

We have presented a computer analysis method for attached egg detection and egg onset event detection. The testing results of egg detection on 100 000 frames and 200 eggs from a variety of mutant types and recording conditions illustrate
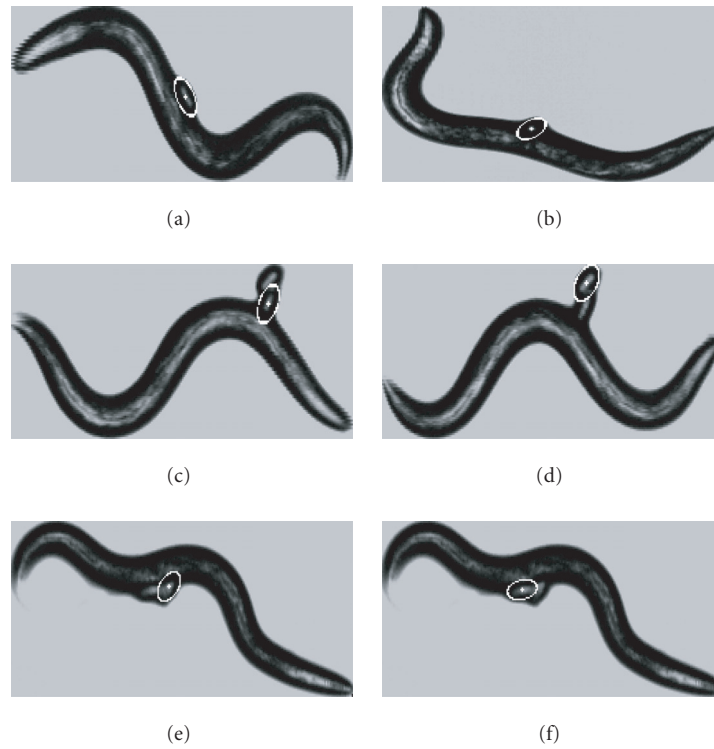
(a)

(b)

(c)

(d)

(e)

(f)

FIGURE 7: Some best-fit results of deformable template matching. Some figures are rotated for plotting. (a) A fully laid egg in perfect condition. (b) A half laid egg. (c), (d) Stacked eggs, identified by repeating the search. (e), (f) Two eggs laid together with close distance.
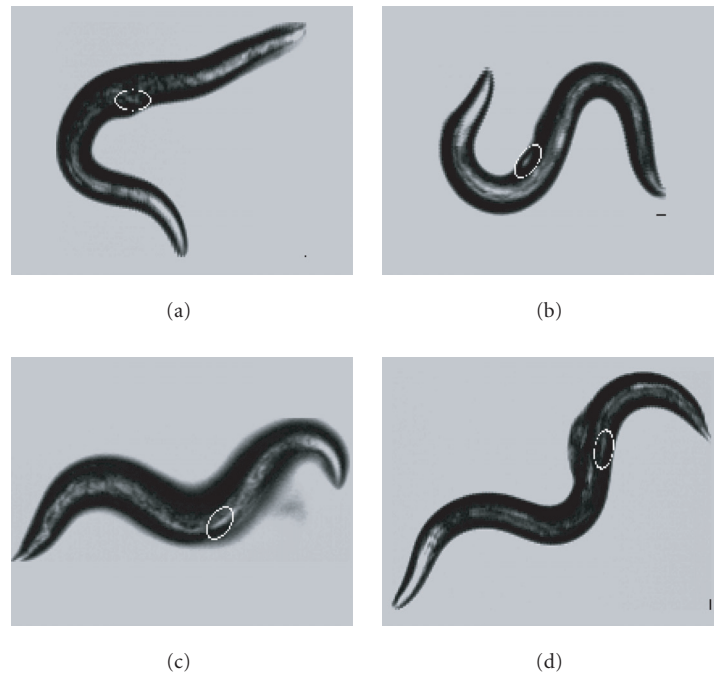

(a)

(b)

(c)

(d)

FIGURE 8: Some nonegg frames that are identified as eggs.

the effectiveness of our proposed algorithm. The behavior study of egg onsets confirms the result from previous studies and shows promise for new findings.

The algorithm proposed is flexible to suit different needs. First, the abnormal width criteria (currently 7.5 pixels/24 μm) can be adjusted accordingly if prior
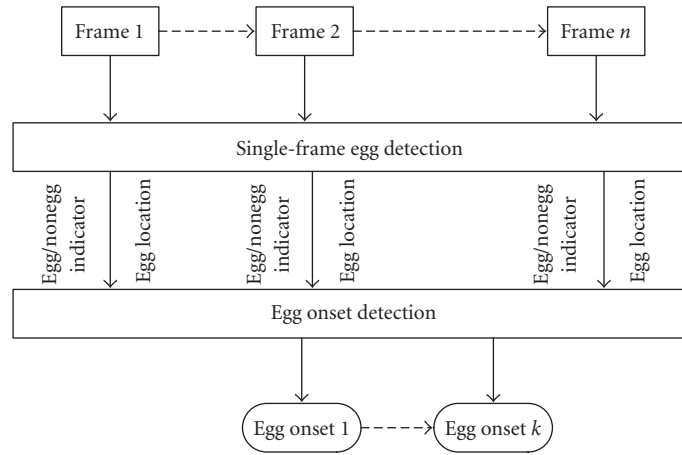
FIGURE 9: Flowchart of egg onset event detection.

TABLE 2: The features which changed significantly 40 seconds before and after egg onsets.

Features	Description
TLMV10MIN	Minimal tail movement in 5 s
TLMV10AVG	Average tail movement in 5 s
HDMV10AVG	Average head movement in 5 s
TLMVHFMIN	Minimal tail movement in 0.5 s
HDMV10MAX	Maximal head movement in 5 s
REVSALTIM	Total percentage of time the worm stays in reversal position
HTBRDMIN	Minimal head and tail area brightness difference
HTBRRMIN	Minimal head/tail brightness
BANGCRMIN	Minimal whole-body-area angle change rate
LNWDRMAX	Maximal length-to-width ratio of the bounding box
BANGCRAVG	Average whole-body-area angle change rate
TLAMPMAX	Maximal amplitude in the tail area
AMPMAX	Maximal amplitude of worm skeleton wave
HDTLANMIN	Minimal head-to-tail angle

knowledge of certain egg size and shape for a particular mutant is present, or the purpose is to obtain a rough idea of whether an egg is present. Secondly, the same applies to the decision criterion t according to the expectation of the false positive and the false negative rate. Third, the current algorithm was applied on videos with frame rate of 2 Hz. The same algorithms can be applied to videos that have different frame rates. With increased frame rates, we anticipate an improved detection result.

With more accurate and complex computer vision systems [4, 5, 6] being developed, we anticipate that many more behavior features will be discovered. Therefore, we will be able to combine the automatic egg onset detection and behavior studies together and explore the temporal correlation between egg laying and other behavioral characteristics more effectively. Moreover, the ability to automatically detect egg-laying events will make it possible to use these correlations between other behaviors and egg laying, which previously could only be assayed through time-consuming human analysis of videotapes [3] as automatically-evaluated features for use in phenotype classification and clustering studies [5].

More generally, egg laying has historically been an extremely useful assay for genetic analysis of diverse aspects of neuromuscular function. For example, egg laying has provided a behavioral measure for the activity of the Go/Gq signaling network in neurons and muscle cells [20] and for neuromodulation by serotonin, acetylcholine, and neuropeptides [7, 21, 22]. The egg-laying assays typically used in genetic studies are generally indirect measures of overall egg-laying rate, and consequently allow limited inference about the functions of specific mutant genes in the behavior. Quantitative assays of the temporal pattern of egg laying can in principle make it possible to distinguish effects on different egg-laying signal transduction pathways [2, 7]. The automated methods for egg detection described here should greatly facilitate these more detailed behavioral analyses.

TABLE 3: The features which changed significantly between 40 seconds before an egg onset and 40 seconds starting from a randomly selected nonegg frame.

Features	Description	Features	Description
HDMVHFMIN	Min. head movt. in 1/2 s	WHRATMIN	Min. width-to-height ratio of MER
HDMVHFMAX	Max. head movt. in 1/2 s	MAJORMIN	Min. length of major axis
HDMVHFAVG	Avg. head movt. in 1/2 s	AMPRMIN	Min. amplitude ratio
HDMV10MAX	Max. head movt. in 5 s	AMPRMAX	Max. amplitude ratio
HDMV10AVG	Avg. head movt. in 5 s	ANCHRMAX	Max. angle change rate
HDMV20MAX	Max. head movt. in 10 s	ANCHSMAX	Max. angle change standard deviation
HDMV20AVG	Avg. head movt. in 10 s	CANGCRMIN	Min. angle change rate in middle sect.
TLMV10MAX	Min. tail movt. in 5 s	CANGCRMAX	Max. angle change rate in middle sect.
TLMV10AVG	Avg. tail movt. in 5 s	CANGCRAVG	Avg. angle change rate in middle sect.
TLMV20AVG	Avg. tail movt. in 10 s	BANGCRMAX	Max. body angle change rate
RV20MAX	Max. reversals in 10 s	HDAMPMIN	Min. amplitude in head
RV20AVG	Avg. reversals in 10 s	TLAMPMAX	Max. amplitude in tail
TOTRV	Total reversals in 5 min	CNTAMPMIN	Min. amplitude in center
REVSALTIM	Total percentage of time the worm stays in reversal position	AVGAMPMIN	Avg. amplitude
TAILBRMIN	Min. tail brightness	HDTLANMAX	Max. head-to-tail angle
TAILBRAVG	Avg. tail brightness	TLANGMAX	Max. head-angle change rate
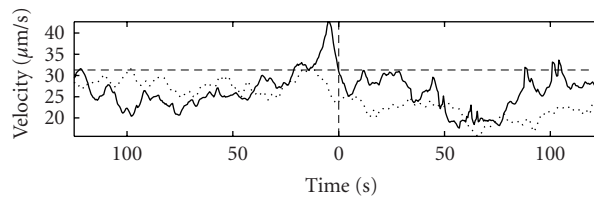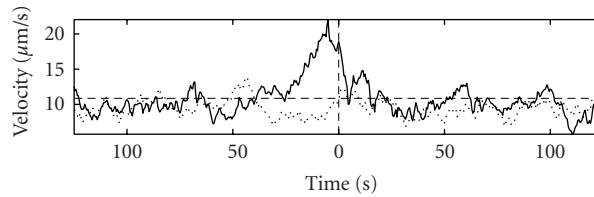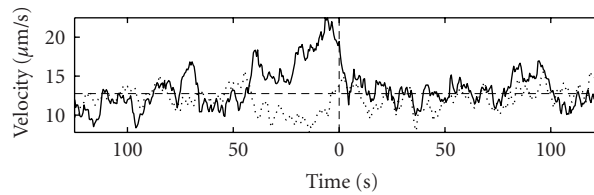
FIGURE 10: Velocity change 125 seconds before and after egg onset. The velocity is a moving average of 10-second interval. (a) Centroid velocity. (b) Head velocity. (c) Tail velocity.

ACKNOWLEDGMENTS

REFERENCES

[1] J. White, E. Southgate, N. Thomson, and S. Brenner, "The structure of the Caenorhabditis elegans nervous system," *Philosophical Transactions of the Royal Society of London. Series B, Biological Sciences*, vol. 314, pp. 1–340, 1986.

[2] L. E. Waggoner, G. T. Zhou, R. W. Schafer, and W. R. Schafer, "Control of alternative behavioral states by serotonin in Caenorhabditis elegans," *Neuron*, vol. 21, no. 1, pp. 203–214, 1998.

[3] L. A. Hardaker, E. Singer, R. Kerr, G. T. Zhou, and W. R. Schafer, "Serotonin modulates locomotory behavior and coordinates egg-laying and movement in Caenorhabditis elegans," *Journal of Neurobiology*, vol. 49, no. 4, pp. 303–313, 2001.

[4] J.-H. Baek, P. Cosman, Z. Feng, J. Silver, and W. R. Schafer, "Using machine vision to analyze and classify Caenorhabditis elegans behavioral phenotypes quantitatively," *Journal of Neuroscience Methods*, vol. 118, no. 1, pp. 9–21, 2002.

[5] W. Geng, P. Cosman, J.-H. Baek, C. C. Berry, and W. R. Schafer, "Quantitative classification and natural clustering of Caenorhabditis elegans behavioral phenotypes," *Genetics*, vol. 165, no. 3, pp. 1117–1126, 2003.

[6] W. Geng, P. Cosman, C. C. Berry, Z. Feng, and W. R. Schafer, "Automatic tracking, feature extraction and classification of C. elegans phenotypes," *IEEE Trans. Biomed. Eng.*, vol. 51, no. 10, pp. 1811–1820, 2004.

[7] L. E. Waggoner, L. A. Hardaker, S. Golik, and W. R. Schafer, "Effect of a neuropeptide gene on behavioral states in Caenorhabditis elegans egg-laying," *Genetics*, vol. 154, no. 3, pp. 1181–1192, 2000.

[8] G. T. Zhou, W. R. Schafer, and R. W. Schafer, "A three-state biological point process model and its parameter estimation," *IEEE Trans. Signal Processing*, vol. 46, no. 10, pp. 2698–2707, 1998.

[9] S. Brenner, "The genetics of Caenorhabditis elegans," *Genetics*, vol. 77, no. 1, pp. 71–94, 1974.

[10] M. Sonka, V. Hlavac, and R. Boyle, *Image Processing, Analysis, and Machine Vision*, Brooks/Cole Publishing Company, Pacific Grove, Calif, USA , Second edition, 1999.

[11] R. Jain, K. Rangachar, and B. Schunck, *Machine Vision*, McGraw-Hill, New York, NY, USA, 1995.

[12] G. Borgefors, "Distance transformations in digital images," *Computer Vision, Graphics, and Image Processing*, vol. 34, no. 3, pp. 344–371, 1986.

[13] T. McInerney and D. Terzopoulos, "Deformable models in medical image analysis: a survey," *Medical Image Analysis*, vol. 1, no. 2, pp. 91–108, 1996.

[14] A. K. Jain, Y. Zhong, and M.-P. Dubuisson-Jolly, "Deformable template models: A review," *Signal Processing*, vol. 71, no. 2, pp. 109–129, 1998.

[15] A. K. Jain, Y. Zhong, and S. Lakshmanan, "Object matching using deformable templates," *IEEE Trans. Pattern Anal. Machine Intell.*, vol. 18, no. 3, pp. 267–278, 1996.

[16] F. Escolano, M. Cazorla, D. Gallardo, and R. Rizo, "Deformable templates for tracking and analysis of intravascular ultrasound sequences," in *Proc. Energy Minimization Methods in Computer Vision and Pattern Recognition (EMMCVPR '97)*, vol. 1223, Venice, Italy, May 1997.

[17] R. Fisker, J. M. Carstensen, M. F. Hansen, F. Bodeker, and S. Morup, "Estimation of nanoparticle size distributions by image analysis," *Journal of Nanoparticle Research*, vol. 2, no. 3, pp. 267–277, 2000.

[18] L. Breiman, J. Friedman, R. Olshen, and C. Stone, *Classification and Regression Trees*, Wadsworth International Group, Belmont, Calif, USA, 1984.

[19] C. E. Metz, "Basic principles of ROC analysis," *Seminars in Nuclear Medicine*, vol. 8, no. 4, pp. 283–298, 1978.

[20] C. A. Bastiani, S. Gharib, M. I. Simon, and P. W. Sternberg, "Caenorhabditis elegans Gq regulates egg-laying behavior via a PLCβ-independent and serotonin-dependent signaling pathway and likely functions both in the nervous system and in muscle," *Genetics*, vol. 165, no. 4, pp. 1805–1822, 2003.

[21] C. Trent, N. Tsung, and H. R. Horvitz, "Egg-laying defective mutants of the nematode Caenorhabditis elegans," *Genetics*, vol. 104, no. 4, pp. 619–647, 1983.

[22] D. Weinshenker, G. Garriga, and J. H. Thomas, "Genetic and pharmacological analysis of neurotransmitters controlling egg-laying in C. elegans," *Journal of Neuroscience*, vol. 15, no. 10, pp. 6975–6985, 1995.

Wei Geng received the B.S. degree in computer science from Beihang University, Beijing, China, in 1993, the M.S. degree from Northeastern University, Boston, Mass, in 1997, and the Ph.D. degree from the University of California, San Diego, Calif, in 2004, both in electrical engineering. From 1993 till 1995, he was a Research Assistant at the National Laboratory on Machine Perception, Peking University, Beijing, China. From 1997 till 2001, he was an Embedded Software Engineer at Hewlett-Packard Company, San Diego, Calif. He was a Senior Analytical Engineer at ID Analytics Inc., San Diego, Calif, in 2004. He is currently a Director of software engineering at Agile systems Inc., San Diego, Calif. His research interests are in the areas of image analysis and embedded software engineering.

Pamela Cosman obtained her B.S. degree with honors in electrical engineering from the California Institute of Technology in 1987, and her M.S. and Ph.D. degrees in electrical engineering from Stanford University in 1989 and 1993, respectively. She was an NSF Postdoctoral Fellow at Stanford University and a Visiting Professor at the University of Minnesota during 1993–1995. In 1995, she joined the faculty of the Department of Electrical and Computer Engineering, the University of California, San Diego, where she is currently a Professor and Codirector of the Center for Wireless Communications. Her research interests are in the areas of image and video compression and processing. She is the recipient of the ECE Departmental Graduate Teaching Award (1996), a Career Award from the National Science Foundation (1996–1999), and a Powell Faculty Fellowship (1997–1998). She was an Associate Editor of the IEEE Communications Letters (1998–2001), a Guest Editor of the June 2000 special issue of the IEEE Journal on Selected Areas in Communications on "error-resilient image and video coding," and was the Technical Program Chair of the 1998 Information Theory Workshop in San Diego. She is currently an Associate Editor of the IEEE Signal Processing Letters and a Senior Editor of the IEEE Journal on Selected Areas in Communications. She is a Member of Tau Beta Pi and Sigma Xi.

Megan Palm is an M.S. student in William Schafer's laboratory at the University of California, San Diego, where she received her B.S. degree. She is currently studying the effects of nicotine on *C. elegans*.

William R. Schafer received the A.B. degree in biology (summa cum laude) from Harvard University, Cambridge, Mass, in 1986, and the Ph.D. degree in biochemistry from the University of California, Berkeley, in 1991. From 1992 till 1995, he was a Life Sciences Research Foundation Postdoctoral Fellow in the Department of Biochemistry and Biophysics, University of California, San Francisco. Since 1995, he has been on the faculty of the Division of Biological Sciences at the University of California, San Diego, where he is currently an Associate Professor and Vice-Chair of neurobiology. His research concerns the molecular and cellular basis for the nervous system function and the relationship between genes and behavior. He is a Member of the Genetics Society of America, the Society for Neuroscience, and the International Society for Neuroethology. He received the John Belling Prize for the outstanding Ph.D. thesis in genetics from UC Berkeley between 1988 and 1993. He also has been the recipient of Young Investigator Awards from the National Alliance for Research on Schizophrenia and Depression and the Beckman Foundation, an Alfred P. Sloan Fellowship, and a Klingenstein Fellowship in Neuroscience. In 2001, he received a Presidential Early Career Award from the National Institutes of Health.